Available online at www.sciencedirect.com
SCIENCE DIRECT
Journal of Power Sources 157 (2006) 153–165
JOURNAL OF POWER SOURCES
www.elsevier.com/locate/jpowsour

Examination of optimal separator shape of polymer electrolyte fuel cell with numerical analysis including the effect of gas flow through gas diffusion layer

Gen Inoue *, Yosuke Matsukuma, Masaki Minemoto

Department of Chemical Engineering, Faculty of Engineering, Kyushu University, Hakozaki, Higashi-ku, Fukuoka 812-8581, Japan

Received 24 May 2005; received in revised form 5 August 2005; accepted 10 August 2005
Available online 15 September 2005

Abstract

This work concentrates on the effects of channel depth and separator shape on cell output performance, current density distribution and gas flow condition in various conditions with PEFC numerical analysis model including gas flow through GDL. When GDL effective porosity was small, the effect of gas flow through GDL which was changed by channel depth on cell output performance became large. However, current density distribution was ununiform. As GDL permeability became larger, cell output density increased, but current density and gas flow rate distribution were ununiform. From the results of changing the gas flow rate, it was found that the ratio of the minimum gas flow rate to the inlet flow rate depended on channel depth. Furthermore, the optimal separator, which increased output density and made the current density distribution and gas flow rate distribution uniform, was examined. It was also found that cell performance had possible to be developed by improving the turning point of the serpentine separator.

Keywords: PEFC; Numerical analysis; Current density distribution; Gas diffusion layer; Pressure drop

1. Introduction

In recent years, humankind has been facing global serious problems of energy and environment. For example, the exhaustion of fossil energy resource, the global warming caused by the green house gas like carbon dioxide, the atmospheric pollution caused by nitrogen oxide, sulfur oxide and particle matter and so on. For the clean and comfortable future, these problems need to be solved immediately. To solve these problems, new energy technologies, which are more efficient, more convenient and cleaner than the current technologies, has been developed. Fuel cell has high power efficiency and enables to reduce the emission of carbon dioxide, because it is different from a thermal power generation or an internal-combustion engine, and converts chemical energy into electric energy directly. And fuel cell can contribute to promote the alternative energy because it can use various fuels, such as a natural gas and methanol. Moreover, it has been effective to conserve the atmosphere because it hardly discharges nitrogen oxide and sulfur oxide. Polymer electrolyte fuel cell (PEFC) is expected as the driving power of vehicles and stationary power supply, because it has low operation temperature and high power density. The development of the components and optimization of the system lead the PEFC performance to improve greatly. However, in order to come it into general use, PEFC greatly needs to be improved the cell performance and durability, and to be reduced the costs. And it is necessary to examine the factor and the mechanism of cell performance and durability by studies in many different fields.

In the internal PEFC, the multi-dimensional phenomena of mass transfer, heat transfer, catalysis, electrochemical reaction and fluid dynamics are caused complexly, and these are strongly related to each other. There are various kinds of studies which examine the internal phenomena of PEFC by

* Corresponding author. Tel.:+81 92 642 3523; fax: +81 92 642 3523.
E-mail address: ginoue@chem-eng.kyushu-u.ac.jp (G. Inoue).

0378-7753/$ – see front matter © 2005 Elsevier B.V. All rights reserved.
doi:10.1016/j.jpowsour.2005.08.003

Nomenclature

b_c	condensation rate constant (s^{-1})
C_j	molar concentration of species j (mol m^{-3})
$C_{j(n)}$	molar concentration of species j in next channel of n direction (mol m^{-3})
$C^e_{O_2}$	oxygen concentration at catalyst layer (mol m^{-3})
$C^{ref}_{O_2}$	reference oxygen concentration (mol m^{-3})
C_p	specific heat at constant pressure (J kg^{-1} K^{-1})
D_j	diffusion coefficient of species j (m^2 s^{-1})
D^{eff}_j	effective diffusion coefficient of species j (m^2 s^{-1})
E	electromotive force (V)
$E_{\Delta H}$	the value of reduction change of water enthalpy to voltage (V)
F	Faraday's constant (96485 C mol^{-1})
h	heat transfer coefficient of gas (J m^{-2} s^{-1} K^{-1})
H_{GDL}	length of GDL gas flow area (m)
ΔH_{H_2O}	change of water enthalpy between vapor and liquid (J mol^{-1})
i	current density (A m^{-2})
i_{O_2}	oxygen exchange current density (A m^{-2})
k	thermal conductivity of solid phase (J m^{-1} s^{-1} K^{-1})
k_p	permeability of GDL (m^2)
k^{sep}	thermal conductivity of separator (J m^{-1} s^{-1} K^{-1})
$l_{d,g}$	gas channel depth (m)
l_{GDL}	GDL thickness (m)
l^{sep}	separator thickness between back plate and gas phase (m)
l^S	thickness of solid phase (m)
M_j	molecular weight of species j (kg mol^{-1})
p	pressure (Pa)
p_n	pressure in next channel of n direction (Pa)
$P_{H_2O,\,sat}$	saturated vapor pressure in stream (Pa)
q_1	heat flux from solid phase to gas phase (J m^{-2} s^{-1})
q_2	heat flux from back plate to gas phase (J m^{-2} s^{-1})
q_3	heat value generated by reaction (J m^{-2} s^{-1})
q_4	heat flux from gas phase to solid phase (J m^{-2} s^{-1})
q_5	heat flux from back plate to solid phase (J m^{-2} s^{-1})
q_6	latent heat value of condensation (J m^{-2} s^{-1})
Q_b	all gas flow rate through GDL per unit volume to next channel (s^{-1})
$Q_{b(n)}$	flow rate through GDL per unit volume to next channel of n direction (s^{-1})
$Q_{b(n,in)}$	inflow rate through GDL per unit volume from next channel of n direction (s^{-1})
$Q_{b(n,out)}$	outflow rate through GDL per unit volume to next channel of n direction (s^{-1})
r_j	molar flux of species j (mol m^{-2} s^{-1})
R	gas constant (8.314 J mol^{-1} K^{-1})
Re	Reynolds number
R_{ohm}	resistance of proton transfer through electrolyte membrane (Ω m^2)
R_{rea}	all reaction rate (s^{-1})
Sc	Schmitt number
Sh	Sherwood number
t	time (s)
T	gas phase temperature (K)
T_n	gas temperature in next channel of n direction (K)
T^b	back plate temperature (K)
T^s	solid phase temperature (K)
U	average gas velocity in GDL of x direction (m s^{-1})
U_T	overall heat transfer coefficient between gas and back plate (J m^{-2} s^{-1} K^{-1})
U^s_T	overall heat transfer coefficient between back plate and solid phase (J m^{-2} s^{-1} K^{-1})
v	flow velocity (m s^{-1})
V	operation voltage (V)
w_C	channel width (m)
w_L	land width (m)
x	distance in x direction (m)
y	distance in y direction (m)

Greek letters

α	net water transfer coefficient
α_t	transfer coefficient
β	parameter in oxygen mass transfer model shown in Table 1
ε	effective porosity of GDL
γ	variable for calculation of overvoltage (A m mol^{-1})
λ	parameter in oxygen mass transfer model
μ	viscosity of mixture gas (Pa s)
ρ	density of mixture gas (kg m^{-3})
ω	parameter in oxygen mass transfer model shown in Table 1

Subscripts

ave	average
H_2O	water
$H_2O(l)$	liquid water
$H_2O(v)$	vapor water
j	species j
N_2	nitrogen
O_2	oxygen
x	x-direction
y	y-direction

Superscripts

a	anode
c	cathode

channel	channel
e	electrode
eff	effective
k	anode or cathode
s	solid phase
sep	separator

unique measurement methods, because it is difficult to measure them directly with an actual cell. Hakenjos et al. [1] visualized the cathode gas channel simultaneously with measurement of current density distribution, and flooding in a gas flow field was examined in various conditions. Kramer et al. [2] examined the relationship between cell output performance and flooding in the gas flow field by a neutron imaging method. On the other hand, there are many studies with numerical analysis. Dutta et al. [3] made a three-dimensional computational model based on a commercial software package (Fluent). Berning and Djilali [4] examined the effect of porosity and thickness of gas diffusion layer (GDL) in a straight channel with the three-dimensional model. Many PEFC numerical analysis models were proposed, and these PEFC numerical analysis models contributed to the optimization of component design and operating condition in a present cell. In our past researches, five kinds of separators were evaluated from the viewpoint of gas flow rate, current density distribution and temperature distribution by a two-dimensional PEFC numerical analysis, which was a heat and flow model of direction to membrane plane [5]. And this model was transformed to a quasi-two-dimensional model including flow and heat transfer of cooling water, and the influence of thickness of membrane and GDL on the cell performance was calculated [6].

On the other hand, Nguyen [7] reported that the oxygen transfer rate to electrode increased and that high output density was obtained with an interdigitated channel which generated gas flow through GDL forcibly. Um and Wang [8] examined gas flow in this interdigitated channel by a numerical analysis. Dohle et al. [9] and Oosthuizen et al. [10] mentioned that there was a possibility that such gas flow through GDL was occurred by large pressure drop in usual serpentine channel shape, and they examined the gas flow rate distribution experimentally and numerically. But current density distribution and the cell performance were not examined in those studies. In our former study [11], two kinds of numerical analysis models were developed step by step. First, GDL mass transfer approximate model based on the theoretical model was developed, and then, PEFC reaction and thermal flow analysis model including gas flow through GDL was developed. Second, These two models were combined, and the effects of separator channel depth on output performance and on current density distribution were examined by this numerical analysis. As a result, it was found that the gas flow rate through GDL, which was caused by the differential pressure between adjoining channels, became larger as channels were shallower. And it was found that the cell output density increased because of gas flow through GDL with shallow gas channel, and that current density distribution became remarkable by ununiform gas flow. In this study, this combined numerical analysis, as mentioned above, allowed to examine the effects of gas flow through GDL on cell output performance, current density distribution and gas flow rate distribution in various conditions: GDL effective porosity, GDL permeability, the cathode gas flow rate and channel shape were changed. Furthermore, in order to make the current density distribution more uniform and to improve the cell output performance, optimal separator shape was examined by the numerical analysis.

2. Numerical analysis model including gas flow through GDL

In other studies which examined concentration and liquid water distribution in GDL by a numerical analysis including gas flow through GDL, the strict analysis model based on CFD with an area of several square millimeters was mainly used. Therefore, from the viewpoint of calculation resources and calculation time, it is difficult to extend this former model which was used in other studies to an actual-sized cell. In our former study [11], the numerical analysis model was separated two models in consideration of practical calculation resources and practical calculation time. First, two-dimensional mass transfer and flow in cathode GDL were calculated, and the effect of gas flow through GDL on oxygen mass transfer rate to electrode was examined under various conditions. This results and theoretical mass transfer model were combined, and the approximate model of oxygen mass transfer in cathode GDL was developed. Second, with this model, the quasi-two-dimensional PEFC reaction and thermal flow analysis model which enabled to calculate an actual-sized cell was made. In this study, the PEFC numerical analysis model that had been developed in our former study [11] was used. This numerical analysis model was developed with the following assumptions:

1. The effective porosity and the permeability of GDL are uniform.
2. The volume of condensation water is ignored in GDL and channels, and water moves with gas.
3. The hydrogen transfer rate in anode GDL is much faster than other mass transfer rates and reaction rates in PEFC and so it is ignored.
4. The reduction of the reaction area caused by flooding of electrode is ignored and the diffusion prevention caused by water condensation is ignored.
5. Gas properties which are density, viscosity and the diffusion coefficient are not uniform actually because the composition is changed locally. However, these values are regarded as constant and uniform for convenience.
6. Cell voltage is uniform.

Table 1
Basic equation of this numerical analysis [11]

Continuity in channel	$\frac{\partial v^{\mathrm{k}}}{\partial x} = -R^{\mathrm{k}}_{\mathrm{rea}} - Q^{\mathrm{k}}_{b}$
Motion in channel	$\rho^{\mathrm{k}} \frac{\mathrm{D}v^{\mathrm{k}}}{\mathrm{D}t} = -\nabla\rho^{\mathrm{k}} + \rho^{\mathrm{k}} v^{\mathrm{k}}(R^{\mathrm{k}}_{\mathrm{rea}} + Q^{\mathrm{k}}_{b}) - 12\mu^{\mathrm{k}} \left(\frac{1}{(l^{\mathrm{k}}_{\mathrm{d,g}})^2} + \frac{1}{(w^{\mathrm{k}}_{\mathrm{C}})^2} \right) v^{\mathrm{k}}$
Mass balance in channel	$\frac{\mathrm{D}C^{\mathrm{k}}_{j}}{\mathrm{D}t} = -\frac{r^{\mathrm{k}}_{j}}{l^{\mathrm{k}}_{\mathrm{d,g}}} + C^{\mathrm{k}}_{j}(R^{\mathrm{k}}_{\mathrm{rea}} + Q^{\mathrm{k}}_{b}) + \sum_{n} C^{\mathrm{k}}_{j(n)} Q^{\mathrm{k}}_{b(n,\mathrm{in})} - \sum_{n} C^{\mathrm{k}}_{j} Q^{\mathrm{k}}_{b(n,\mathrm{out})}$
Energy in channel	$\frac{\mathrm{D}T^{\mathrm{k}}}{\mathrm{D}t} = \frac{q^{\mathrm{k}}_{1}+q^{\mathrm{k}}_{2}}{\rho^{\mathrm{k}} C^{\mathrm{k}}_{\mathrm{p}} l^{\mathrm{k}}_{\mathrm{d,g}}} + T^{\mathrm{k}}(R^{\mathrm{k}}_{\mathrm{rea}} + Q^{\mathrm{k}}_{b}) + \sum_{n} T^{\mathrm{k}}_{n} Q^{\mathrm{k}}_{b(n,\mathrm{in})} - \sum_{n} T^{\mathrm{k}}_{n} Q^{\mathrm{k}}_{b(n,\mathrm{out})}$
Energy in MEA and GDL	$\rho^{\mathrm{s}} C^{\mathrm{s}}_{\mathrm{p}} \frac{\partial T^{\mathrm{s}}}{\partial t} = k^{\mathrm{s}} \nabla^2 T^{\mathrm{s}} + \frac{q^{\mathrm{s}}_{3}+q^{\mathrm{s}}_{4}+q^{\mathrm{s}}_{5}+q^{\mathrm{s}}_{6}}{l^{\mathrm{s}}}$
Gas flow rate through GDL	$Q^{\mathrm{k}}_{b(n)} = \frac{k_{\mathrm{p}}}{\mu^{\mathrm{k}}} \frac{l^{\mathrm{k}}_{\mathrm{GDL}}}{l^{\mathrm{k}}_{\mathrm{d,g}} w^{\mathrm{k}}_{\mathrm{C}} w^{\mathrm{k}}_{\mathrm{L}}} (p^{\mathrm{k}} - p^{\mathrm{k}}_{n}), \quad Q^{\mathrm{k}}_{b} = \sum_{n} Q^{\mathrm{k}}_{b(n)}$
Reaction rate	$r^{\mathrm{a}}_{\mathrm{H_2}} = \frac{i}{2F}, \quad r^{\mathrm{a}}_{\mathrm{H_2O(v)}} = \alpha \frac{i}{F} + l^{\mathrm{a}}_{\mathrm{d,g}} b_{\mathrm{c}} \left(C^{\mathrm{a}}_{\mathrm{H_2O(v)}} - \frac{P^{\mathrm{a}}_{\mathrm{H_2O,sat}}}{RT^{\mathrm{a}}} \right), \quad r^{\mathrm{a}}_{\mathrm{N_2}} = 0$
	$r^{\mathrm{c}}_{\mathrm{O_2}} = \frac{i}{4F}, \quad r^{\mathrm{c}}_{\mathrm{H_2O(v)}} = -(1+2\alpha)\frac{i}{2F} + l^{\mathrm{c}}_{\mathrm{d,g}} b_{\mathrm{c}} \left(C^{\mathrm{c}}_{\mathrm{H_2O(v)}} - \frac{P^{\mathrm{c}}_{\mathrm{H_2O,sat}}}{RT^{c}} \right), \quad r^{\mathrm{c}}_{\mathrm{N_2}} = 0$
	$r^{\mathrm{a}}_{\mathrm{H_2O(l)}} = -l^{\mathrm{a}}_{\mathrm{d,g}} b_{\mathrm{c}} \left(C^{\mathrm{a}}_{\mathrm{H_2O(v)}} - \frac{P^{\mathrm{a}}_{\mathrm{H_2O,sat}}}{RT^{\mathrm{a}}} \right), \quad r^{\mathrm{c}}_{\mathrm{H_2O(l)}} = -l^{\mathrm{c}}_{\mathrm{d,g}} b_{\mathrm{c}} \left(C^{\mathrm{c}}_{\mathrm{H_2O(v)}} - \frac{P^{\mathrm{c}}_{\mathrm{H_2O,sat}}}{RT^{\mathrm{c}}} \right)$
	$R^{\mathrm{k}}_{\mathrm{rea}} = \frac{1}{l^{\mathrm{k}}_{\mathrm{d,g}} \rho^{\mathrm{k}}} \sum_{j} M_j r^{\mathrm{k}}_{j}$
Heat flux	$q^{\mathrm{k}}_{1} = h^{\mathrm{k}}(T^{\mathrm{s}} - T^{\mathrm{k}}), \quad q^{\mathrm{k}}_{2} = U^{\mathrm{k}}_{T}(T^{b} - T^{\mathrm{k}}), \quad q^{\mathrm{s}}_{3} = (E_{\Delta H} - V)_i$ $q^{\mathrm{s}}_{4} = h^{\mathrm{a}}(T^{\mathrm{a}} - T^{\mathrm{s}}) + h^{\mathrm{c}}(T^{\mathrm{c}} - T^{\mathrm{s}}), \quad q^{\mathrm{s}}_{5} = U^{\mathrm{s(a)}}_{T}(T^{b} - T^{\mathrm{s}}) + U^{\mathrm{s(c)}}_{T}(T^{b} - T^{\mathrm{s}})$ $q^{\mathrm{s}}_{6} = -\Delta H_{\mathrm{H_2O}}(r^{\mathrm{a}}_{\mathrm{H_2O(l)}} + r^{\mathrm{c}}_{\mathrm{H_2O(l)}})$ $U^{\mathrm{k}}_{T} = \frac{1}{\frac{1}{h^{\mathrm{k}}} + \frac{l^{\mathrm{sep}}}{k^{\mathrm{sep}}}}, \quad U^{\mathrm{s(k)}}_{T} = \frac{k^{\mathrm{sep}}}{l^{\mathrm{sep}} + l^{\mathrm{k}}_{\mathrm{d,g}}}$
Current density	$V = E - \frac{RT}{\alpha_{\mathrm{t}} 2F} \ln \left[\frac{i C^{\mathrm{ref}}_{\mathrm{O_2}}}{i_{\mathrm{O_2}} C^{\mathrm{e}}_{\mathrm{O_2}}} \right] - R_{\mathrm{ohm}} i, \quad \gamma = \frac{i_{\mathrm{O_2}}}{C^{\mathrm{ref}}_{\mathrm{O_2}}}$
Oxygen mass transfer in GDL	(up-stream) $Sh = \beta + \lambda Re^{0.5} Sc^{0.8}$ (down-stream) $Sh = \beta + \lambda (Re - \omega)^{0.5} Sc^{0.5}$ $Sh = \frac{i}{4F} \frac{l_{\mathrm{GDL}}}{D^{\mathrm{eff}}_{\mathrm{O_2}} (C^{\mathrm{channel}}_{\mathrm{O_2}} - C^{\mathrm{e}}_{\mathrm{O_2}})}, \quad Re = \frac{l_{\mathrm{GDL}} \rho U}{\mu}, \quad Sc = \frac{\mu}{\rho D^{\mathrm{eff}}_{\mathrm{O_2}}}$ $\lambda = \frac{1}{2} \sqrt{\frac{l_{\mathrm{GDL}}}{\pi H_{\mathrm{GDL}}}}, \quad D^{\mathrm{eff}}_{j} = \varepsilon D_j$

7. The inlet gas flow rate in each channel is uniform.
8. Fluid is incompressible Newtonian fluid and ideal gas. Flow condition is laminar flow.
9. The temperature of a back plate is uniform and constant.
10. Heat transfer between a separator and gas is ignored. But heat transfer among a gas phase, a solid phase and a back plate is included.
11. Only resistance overvoltage and water transfer in membrane include the influence of temperature.
12. In a membrane, ionic conductivity, the electro-osmosis coefficient and the water effective diffusion coefficient that depend on membrane humidity are determined by water activity of the anode side.
13. The gas cross-over through a membrane is disregarded.

The basic equations and the schematic analysis model are shown in Table 1 and Fig. 1, respectively. The derivations of these basic equations were shown in Ref. [11], but it was omitted in this study. In Table 1, the equation of oxygen mass transfer in GDL is original and the most important.

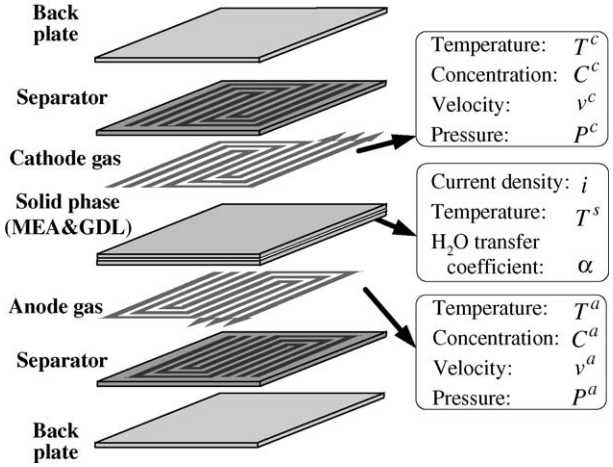

Fig. 1. Model of numerical analysis.

In our former study, the approximate equation of the oxygen mass transfer rate to electrode through GDL, which was the function of Reynolds number and Schmitt number and was in proportion to the square root of Reynolds number, was obtained with a numerical analysis and a theoretical model. In its equations shown in Table 1, it was found that β was 0.624 and ω was 1.3 when width of channel and land were both 1 mm and thickness of GDL was 300 μm. By using this approximate equations of oxygen mass transfer in GDL, the internal phenomena of actual size cell, for example, the current density distribution and the gas flow rate distribution, were examined with numerical analysis in realistic calculation time.

Though the separator shape was a two-dimensional structure to the direction of the membrane faces, the quasi-two-dimensional analysis model was made by assuming the direction from the inlet to the outlet to be a positive x-direction in each channel and by making a channel meander. And in order to calculate gas flow rate that flowed to the next channel through GDL, pressure distribution was calculated by the two-dimensional analysis. Flow, concentration and temperature in anode and cathode channel were calculated with the equations of momentum, mass balance and energy, respectively. The equation of motion took into consideration the gas flow through GDL, which was calculated by the differential pressure between adjoining channels. The temperature of membrane and GDL was assumed to be the same as each other, and those temperature distributions of the direction of membrane face was calculated. The current density was calculated with the oxygen mass transfer model and the overvoltage equation which were substituted for the following three local factors: concentration of oxygen and hydrogen and vapor, temperature of a membrane and anode gas and cathode gas and the gas flow velocity in GDL. The reaction rate was calculated with local current density. With this reaction rate, flow, concentration and temperature were calculated again. Such series of calculations were repeated until all variables became constant; the relative error of all mass and energy balances of the inflow rate, the outflow rate and the variation in cell became less than 1%.

3. Comparison of calculation results with experimental results

In order to confirm the validity of this numerical analysis model, the i–V characteristic of a 25 cm^2 cell was examined by experiments and a numerical analysis. The anode and cathode separators had five serpentine channels for each, and the channel width, the land width and the channel depth were all 1 mm. The thickness of membrane and GDL were 15 μm and 300 μm. The supplied gases were air and pure hydrogen. These gases flowed through a humidifier and to the cell set in a thermostat. The thermostat and the humidifier were controlled at 60 °C. In all experiments, it was confirmed that the change of back plate temperature was within 3 °C by thermocouples. The anode gas flow rate was 300 $cm^3\ min^{-1}$, and the cathode gas flow rate was controlled between 400 $cm^3\ min^{-1}$ and 800 $cm^3\ min^{-1}$ every 100 $cm^3\ min^{-1}$. And the differential pressure between an inlet and an outlet of the cell was measured during measuring the current density and voltage. If liquid water does not exist in a gas channel and does not inhibit the gas flow, it is thought that the pressure drop was in proportion to the gas flow rate in laminar flow condition, and that the pressure drop divided by the gas flow rate was constant. It was confirmed that the value was almost constant, and that gas flow was not inhibited by liquid water under all flow conditions. In this calculation, the GDL effective porosity, which was used to calculate the oxygen mass transfer rate to the electrode in GDL, was determined by fitting the calculation results to the experimental results in all gas flow rate conditions. Fig. 2 shows the experimental results and the calculation results that GDL effective porosity is 0.11. In this figure, although there was small difference between each other in the middle current density, it could be confirmed that the calculation results mostly agreed with the experimental results. Although an actual porosity of GDL in our cell is about 0.7, the GDL effective porosity, which was determined by fitting the calculation results to the experimental results, was less than that value. It is considered that the difference was caused because of the liquid water in GDL and the inappropriateness of mass transfer model in GDL with Fick's equation. Though the mass transfer model without fitting the calculation results to the experimental results needs to be developed in order to calculate in various operating conditions, in this study, the GDL effective porosity was set about 0.1–0.2 in the calculations in Section 4 for convenience.

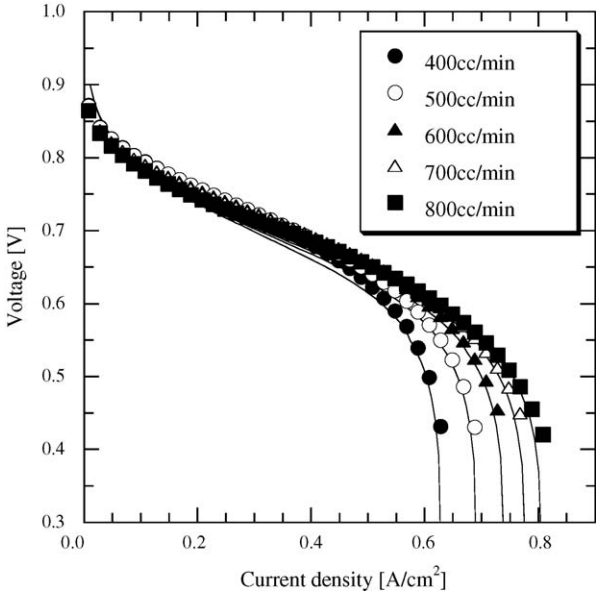

Fig. 2. Comparison of experimental results with calculation results.

4. Calculation results and discussion

The influence of gas flow through GDL on cell performance was examined with this numerical analysis model including the gas flow through GDL. Table 2 shows the calculation parameter including the operating condition and the dimensions of MEA, GDL and a separator. It was supposed that physical properties were constant, because the effect of changing gas composition in a cell on physical properties was very little. In this study, the GDL effective porosity, the GDL permeability and the cathode gas flow rate were changed, and the basic condition was as follows: GDL effective porosity was 0.2, GDL permeability was 2.5×10^{-11} m^2, the cathode gas flow rate was 1.5×10^4 cm^3 min^{-1}. Furthermore, the influence of separator shape on cell performance was examined. Fig. 3 shows the separator shape of the anode side and the cathode side that is a target of this study. The electrode area was a 150 mm^2. The width of a channel and a land were all 1 mm, and there were 15 channels in the separators A and B, and 25 channels in the separators C and D. The difference between separators A and B was the number of channels turned in a bundle, and the difference between separators C and D was the same as that of separators A and B. Separators A and C are expressed as an ordinary serpentine separator, and separators B and D are expressed as a distributed serpentine separator in this paper. The effect of the shape of the cathode separator was examined in this study. The anode separator was fixed to separator A. The basic cathode separator shape was separator A. The anode gas flow pattern and the cathode gas flow pattern were counter flow as Fig. 1. In order to examine the characteristic of current density–cell voltage at each condition, the calculation was carried out from 0.9 V to 0.05 V every 0.05 V.

4.1. Effect of GDL porosity on cell performance and gas flow condition

First, the effect of GDL porosity on cell performance was examined. Fig. 4 shows the effects of GDL porosity and channel depth on a current density–voltage curve. In this graph,

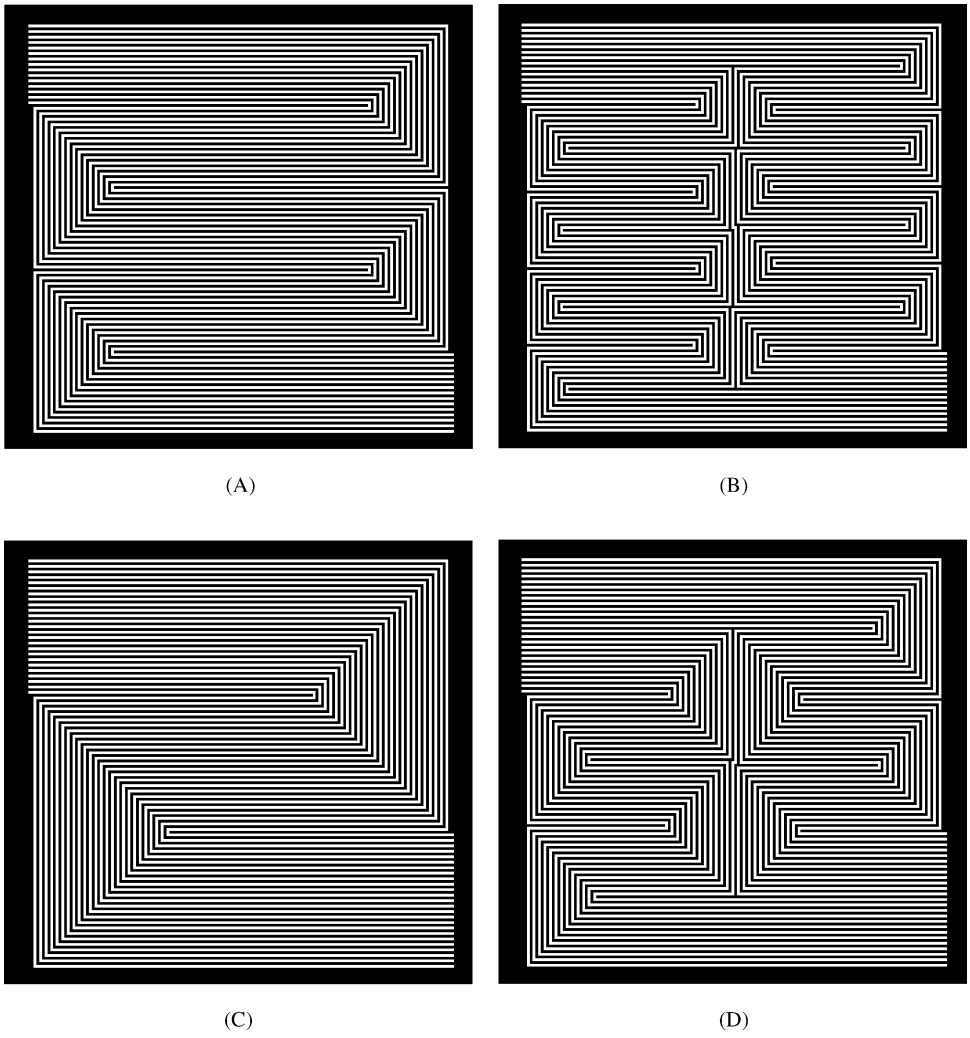

Fig. 3. Separator shape: (A) the ordinary serpentine separator with 15 channels; (B) the distributed serpentine separator with 15 channels; (C) the ordinary serpentine separator with 25 channels; (D) the distributed serpentine separator with 25 channels.

Table 2
Operation condition and shape of cell

Pressure (MPa)	0.1
Inlet gas and humidify temperature (°C)	60
Back plate temperature (°C)	60
Inlet gas composition	
Anode	Pure H_2
Cathode	Air (O_2:N_2 = 21:79)
Inlet anode gas flow rate ($m^3\ s^{-1}$)	16.67×10^{-5}
Thickness of membrane (μm)	30
Size of catalyst layer (cm^2)	225
GDL thickness (μm)	300
Channel width (mm)	1
Land width (mm)	1
Transfer coefficient	0.3
Electromotive force	1.23 V
γ for calculation of overvoltage ($A\ m\ mol^{-1}$)	4.0×10^{-2}
Operated variable parameter[a]	
Channel depth (mm)	0.5, 1.0, 1.5
GDL effective porosity	0.1–0.2
GDL permeability (m^2)	2.5×10^{-11} to 2.5×10^{-10}
Inlet cathode gas flow rate ($m^3\ s^{-1}$)	6.25×10^{-5} to 25.00×10^{-5}
Number of the channel	15 or 25

[a] The underlined values are basic condition.

it is found that the output density increased as the channel was shallower, and that the influence of the channel depth was larger as the GDL effective porosity was reduced. The pressure drop in a gas channel became larger as the channel was shallower, and the differential pressure between adjoining channels increased. As a result, the gas flow rate through GDL increased, and the oxygen mass transfer rate to electrode through GDL also increased. And as the oxygen mass transfer rate in GDL was influential in all PEFC reactions and mass transfer process, the influence of the channel depth was large. Fig. 5 shows the effect of GDL porosity and channel depth on current density distribution at 0.6 V. Fig. 5(a–c) shows the current density distribution with effective porosity 0.2 and channel depth 0.5 mm, 1.0 mm and 1.5 mm, respectively.

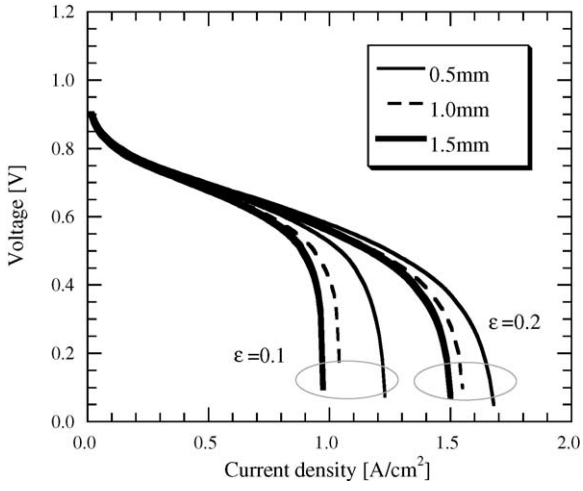

Fig. 4. Effect of GDL porosity and channel depth on current density–voltage curve.

Similarly, Fig. 5(d–f) shows the results with effective porosity 0.1. In these graphs, the current density at the turning sections in a channel was higher than that at other sections. Because the gas flow rate through GDL at the turning sections, which was caused by the differential pressure between adjoining channels, was larger than other sections. The unevenness of current density distribution with shallow channels was large, and moreover the unevenness was remarkable for the low effective porosity. In order to evaluate the current density distribution quantitatively, the difference between the maximum current density and the minimum current density at the average current density $0.6\ A\ cm^{-2}$ was calculated in each calculation condition. Fig. 6 shows the relationship among the value and the effective porosity and the channel depth. In this graph, it was found that the influence of the channel depth on the current density distribution, which was caused by the ununiform gas flow rate distribution, increased with the reduction of the effective porosity. Although the direct causal relationship between the current density distribution and the durability of cell was not grasped very well, it is thought that the current density distribution causes the temperature distribution and the relative humidity distribution. The electrolyte membrane has the role to conduct the proton and to separate the both reactant gases, and in the case of the general electrolyte membrane, the property of membrane is affected by the water content. Therefore, it is thought that the current density distribution must be as uniform as possible in order to keep the membrane moist uniform and sufficient.

4.2. *Effect of GDL permeability on cell performance and gas flow condition*

In our former study [11], when the GDL permeability was $2.5 \times 10^{-11}\ m^2$, it was confirmed that the calculation results agreed with the experimental results about gas flow. In this study, this permeability was changed between $2.5 \times 10^{-11}\ m^2$ and $2.5 \times 10^{-10}\ m^2$ in order to examine the effect of GDL permeability on cell performance, and gas flow condition was examined. Fig. 7 shows the effect of GDL permeability on current density-voltage curve in the case of 1 mm depth channels (kp_1 equals $2.5 \times 10^{-11}\ m^2$). In this graph, it is found that the output density increased with increasing permeability. This result was caused by the increase of the gas flow rate through GDL, too. Fig. 8 shows the pressure distribution when the GDL permeability was $2.5 \times 10^{-11}\ m^2$ (a) and it was $2.5 \times 10^{-10}\ m^2$ (b), and the pressure at the outlet was a reference value. In this graph, it was found that the pressure distribution was different at each permeability, and that the overall pressure drop of a cell decreased with increasing permeability. As the gas flow rate through GDL increased in comparison with the gas flow rate in a channel, the gas flow condition was transformed from the condition that gas flowed uniformly in the bundled serpentine channel to the condition that the gas flowed in a diagonal direction of an electrode area through GDL. The gas flow rate in channels was in proportion to the pressure gradient at each point in the

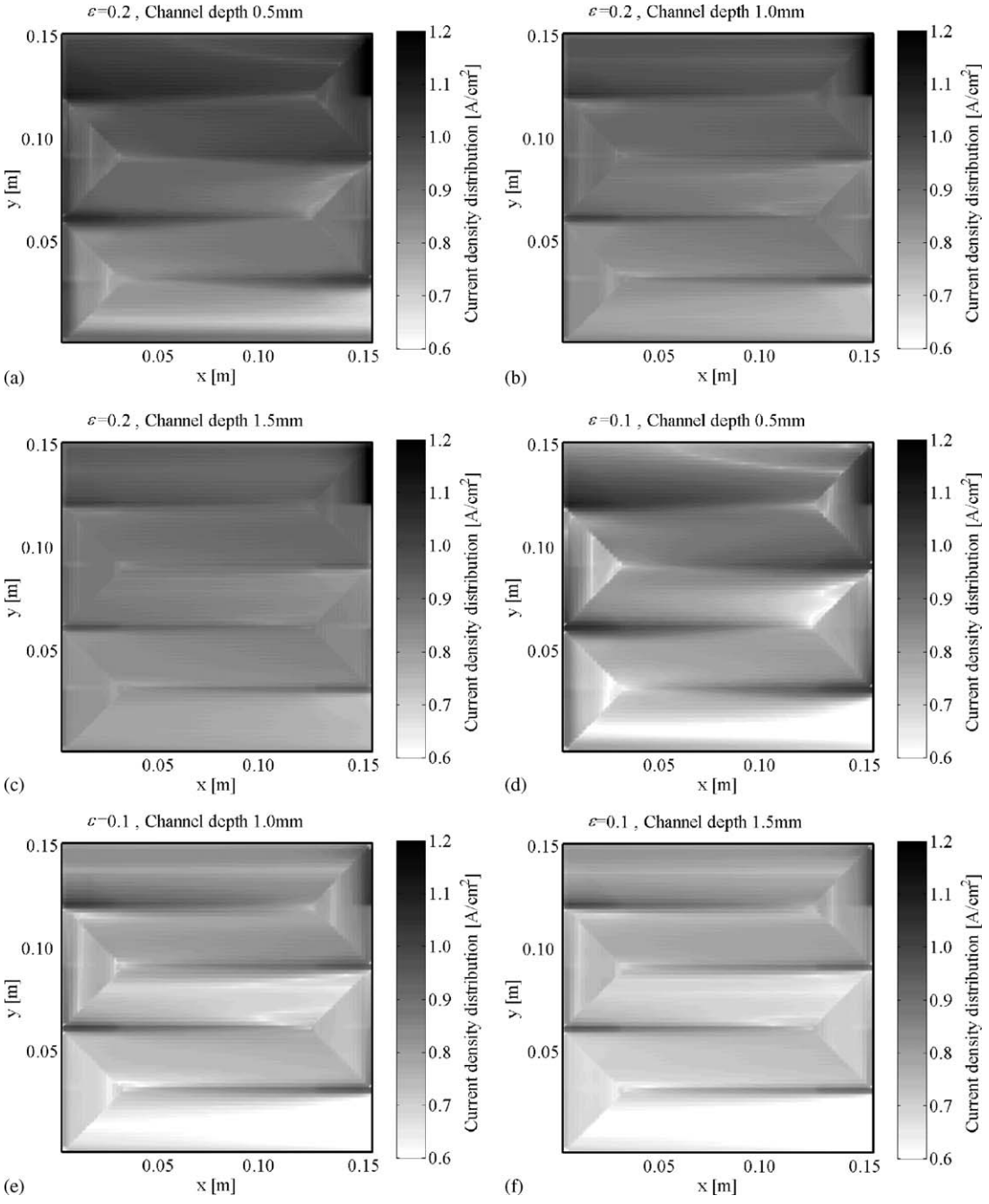

Fig. 5. Current density distribution with each GDL effective porosity and channel depth at 0.6 V.

graph, and comparing Fig. 8(A) with Fig. 8(B), it was found that the pressure gradient of Fig. 8(B) was gentle all over the cell and that the gas flow rate in channels decreased. Fig. 9 shows the effect of GDL permeability and channel depth on the rate of the minimum flow velocity to inlet velocity. When the gas flow rate through GDL was zero, the minimum flow velocity in gas channel divided by the inlet flow rate equals to one. In the case that the channel depth was 1.0 mm, the ratio of the minimum gas velocity was lower than that of the 1.5 mm depth channel. From this result, it was found that the local reduction of gas flow velocity was affected by the biased gas flow condition with gas flow through GDL. And as the permeability was larger and the gas flow filed in GDL influenced more strongly on the overall cell gas flow condition, the influence of channel depth on overall gas flow condition was lower.

4.3. Effect of gas flow rate on cell performance and gas flow condition

Next, the effect of gas flow rate on cell performance was examined. Fig. 10 shows the effect of cathode gas flow rate

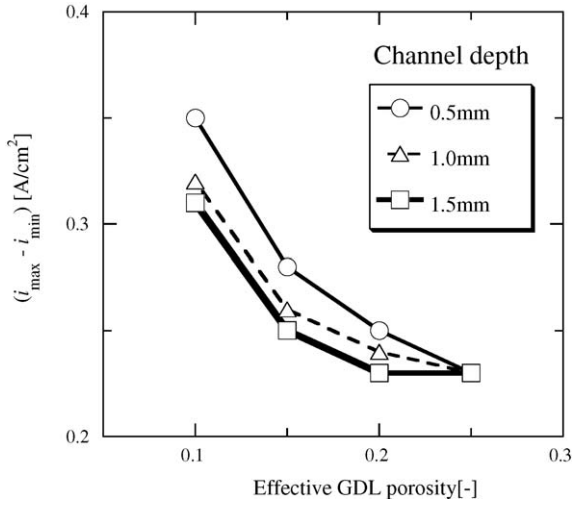

Fig. 6. Effect of GDL porosity and channel depth on the difference between the maximum current density and the minimum current density at the average current density 0.6 A cm^{-2}.

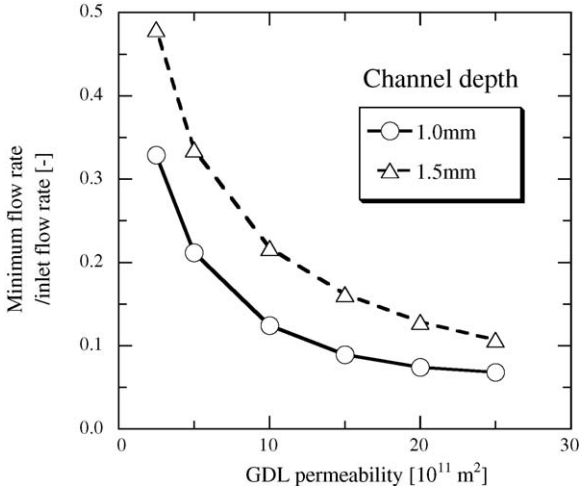

Fig. 9. Effect of GDL permeability and channel depth on the rate of the minimum flow velocity to the inlet velocity.

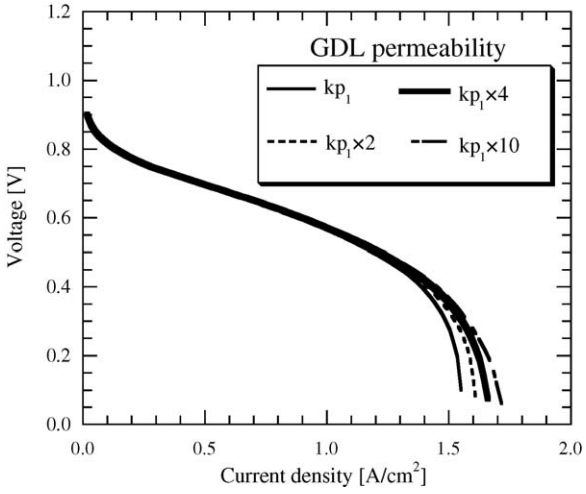

Fig. 7. Effect of GDL permeability on current density–voltage curve.

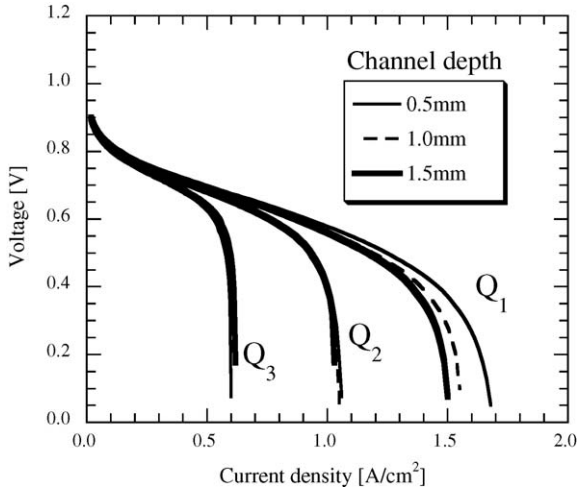

Fig. 10. Effect of gas flow rate and channel depth on current density–voltage curve (Q_1 is 1.50×10^4 cm^3 min^{-1}, Q_2 is 0.75×10^4 cm^3 min^{-1}, Q_3 is 0.375×10^4 cm^3 min^{-1}).

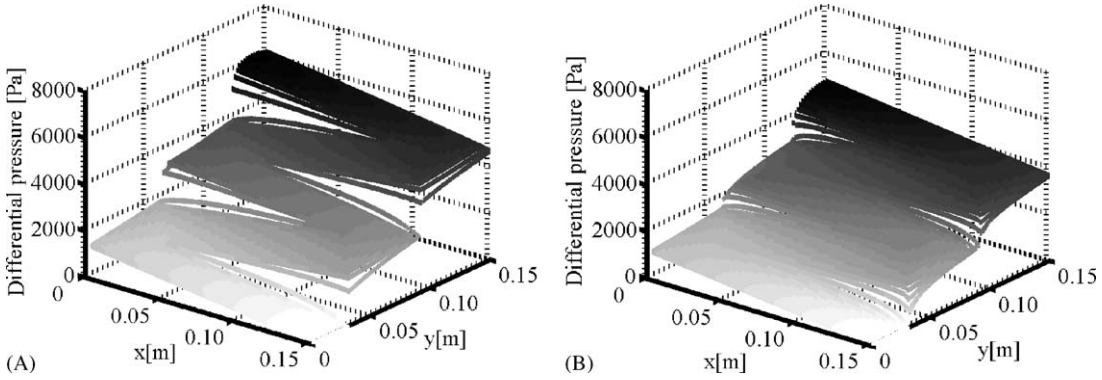

Fig. 8. Pressure distribution in case the GDL permeability was 2.5×10^{-11} m^2 (A) and it was 2.5×10^{-10} m^2 (B).

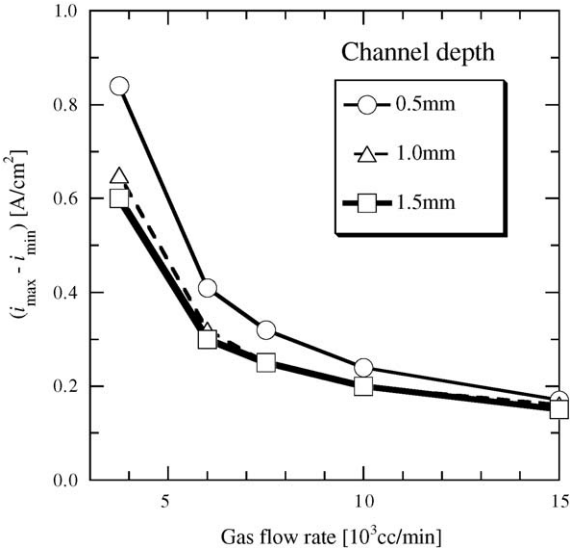

Fig. 11. Effect of gas flow rate and channel depth on the difference of between the maximum current density and the minimum current density.

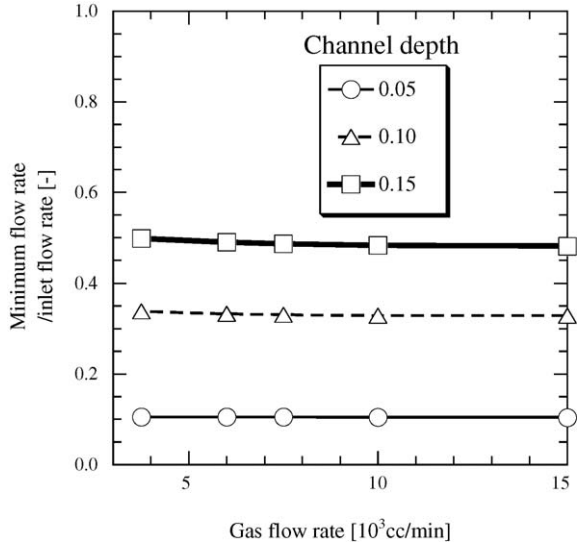

Fig. 12. Effect of gas flow rate and channel depth on the rate of the minimum flow velocity to the inlet velocity.

and channel depth on current density–voltage curve. As the cathode gas flow rate was lower, the influence of the channel depth on cell output performance was lower. It was found that the cell output performance increased by the gas flow through GDL when the oxygen utilization was low and enough oxygen was supplied. Fig. 11 shows the effect of the gas flow rate and channel depth on the difference of between the maximum current density and the minimum current density at 0.5 A cm^{-2} which was the average current density. In this graph, when the gas flow rate was low and the oxygen utilization was high, the current density distribution, which was caused by the oxygen concentration distribution, became more ununiform. And as the gas flow channel was shallower, the current density distribution was larger. These results were also caused by the gas flow through GDL. Fig. 12 shows the effect of the gas flow rate and channel depth on the rate of the minimum flow velocity to an inlet velocity. It was found that the ratio of the gas flow velocity distribution of each channel depth was independent of the gas flow rate, and that it depended on the channel shape and GDL permeability. This result was very interesting. Generally, the gas velocity was risen by making the gas channel shallower for improving the mobility of liquid water. However, it was inferred from this result that the minimum gas velocity with shallow channels might be lower than that with deep channels by the gas flow through GDL. Actually, when the cathode gas flow rate was 7.5×10^3 cm^3 min^{-1}, the minimum gas velocity with the channel depth of 0.5 mm, 1.0 mm and 1.5 mm were 1.75 m s^{-1}, 2.76 m s^{-1} and 2.70 m s^{-1}, respectively. And the minimum gas velocity of the 1.0 mm channel was the largest. Consequently, from the viewpoint of the mobility of the liquid water, this numerical analysis model was very applicable to know the gas flow condition in a cell.

4.4. *Effect of separator shape on cell performance and gas flow condition*

In the former sections, the effect of GDL effective porosity, permeability and gas flow rate on the cell performance was examined by the numerical analysis including the gas flow through GDL. And the followings were found: as the gas flow through GDL increased, the cell output performance was higher by improving the oxygen mass transfer in GDL, and the current density distribution was more ununiform because of the complicated gas flow condition in GDL and channels. These results were obtained when the cathode separator was Fig. 3(A). Therefore, in this study, the optimal separator shape which made the output density increase and made the current density distribution more uniform was examined by the numerical analysis. Fig. 13 shows the effect

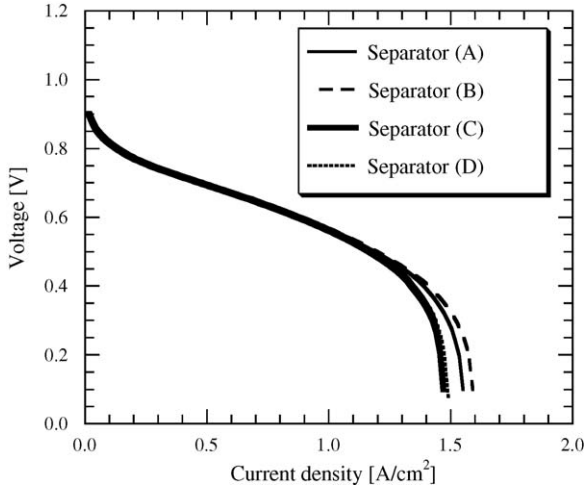

Fig. 13. Effect of separator shape on current density–voltage curve.

of the separator shape on current density–voltage curve of each separator shape of Fig. 3 with a 1 mm depth channel. In this figure, it was found that the cell voltage of separators A and B with 15 channels were higher than that of separators C and D with 25 channels at the high current density section. Because the differential pressure between adjoining channels of separators A and B were larger than that of separators C and D for the difference of gas flow rate per channel. The oxygen mass transfer rate to electrode, which was shown in Table 1, was in proportion to the square root of the gas flow velocity through GDL. The effect of gas flow velocity through GDL was decreased as the velocity increased. Therefore, it was expected that the oxygen transfer rate and the cell output in overall cell increased by distributing the turning section of separator and by making a little cathode gas flow through GDL in many sections. In this graph, it was found that the cell voltage of separators B and D of which the turning sections were distributed were higher than that of separators A and C which had the ordinary serpentine channels, and the effectiveness of the separator shape which controlled the gas flow through GDL was confirmed. Judging from Fig. 4, this difference of each separator was large in the operating condition that the GDL effective porosity was lower. Fig. 14 shows the current density distribution of each separator shape at 0.6 V. The current density distribution of separators B and D were more uniform than that of separators A and C. Fig. 15 shows the pressure distribution with each separator shape. The unevenness of the differential pressure between adjoining channels of ordinary serpentine separators (A and C) was larger than that of distributed serpentine separators (B and D). The ununiform current density distribution was caused by the uneven gas flow condition, and it was thought that it had to be uniform from the viewpoint of the durability. Concerning this point, it was found that the distributed serpentine separator was better. Fig. 16 shows the effect of separator shape on the rate of the minimum gas flow velocity to the inlet gas velocity. As the channel was shallower, the local decrement of gas velocity in each separator was remarkable. And the minimum gas flow velocity with distributed serpentine channel was bigger than that with ordinary serpentine channel, as a result, it was inferred that the distributed serpentine separator was effective in order to raise the mobility of liquid water. As mentioned above, the distributed serpentine separator was excellent for increasing the cell output performance and the mobility of liquid water, and for making current density

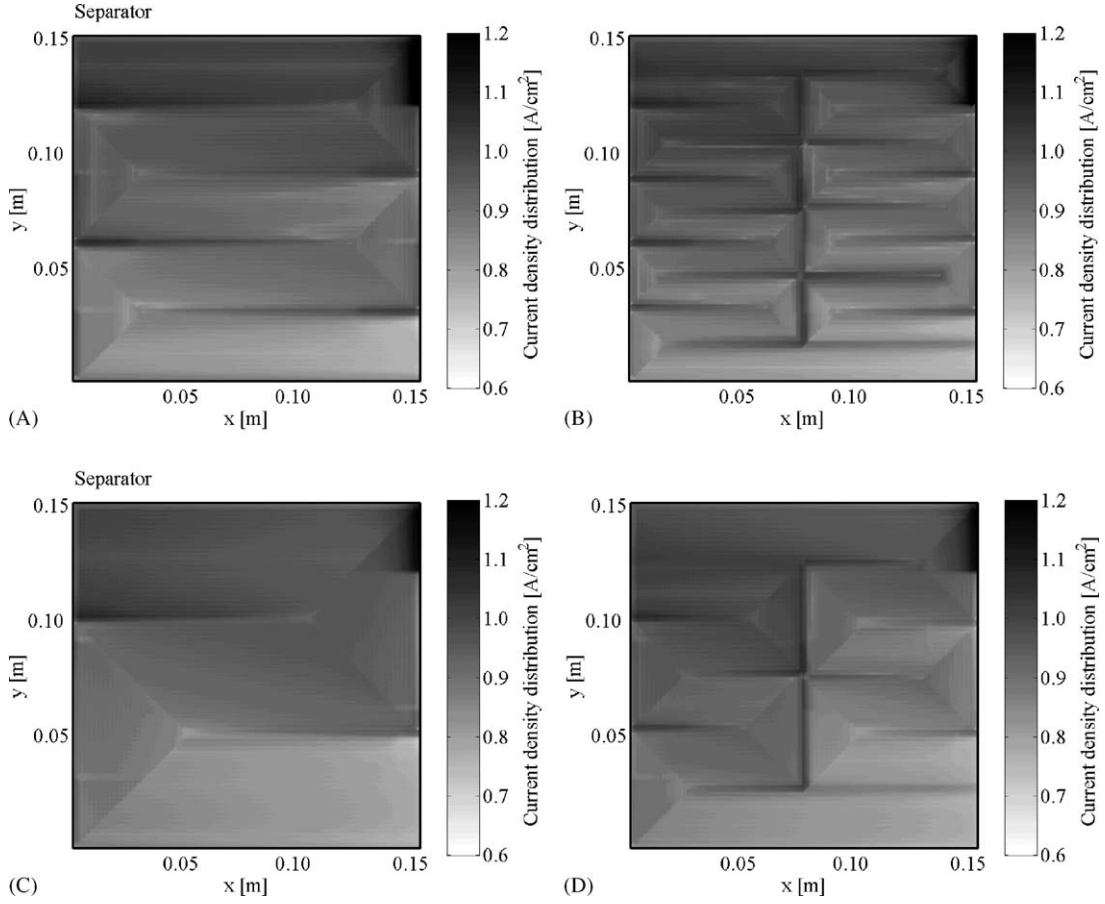

Fig. 14. Current density distribution with each separator shape at 0.6 V (channel depth was 1.0 mm).

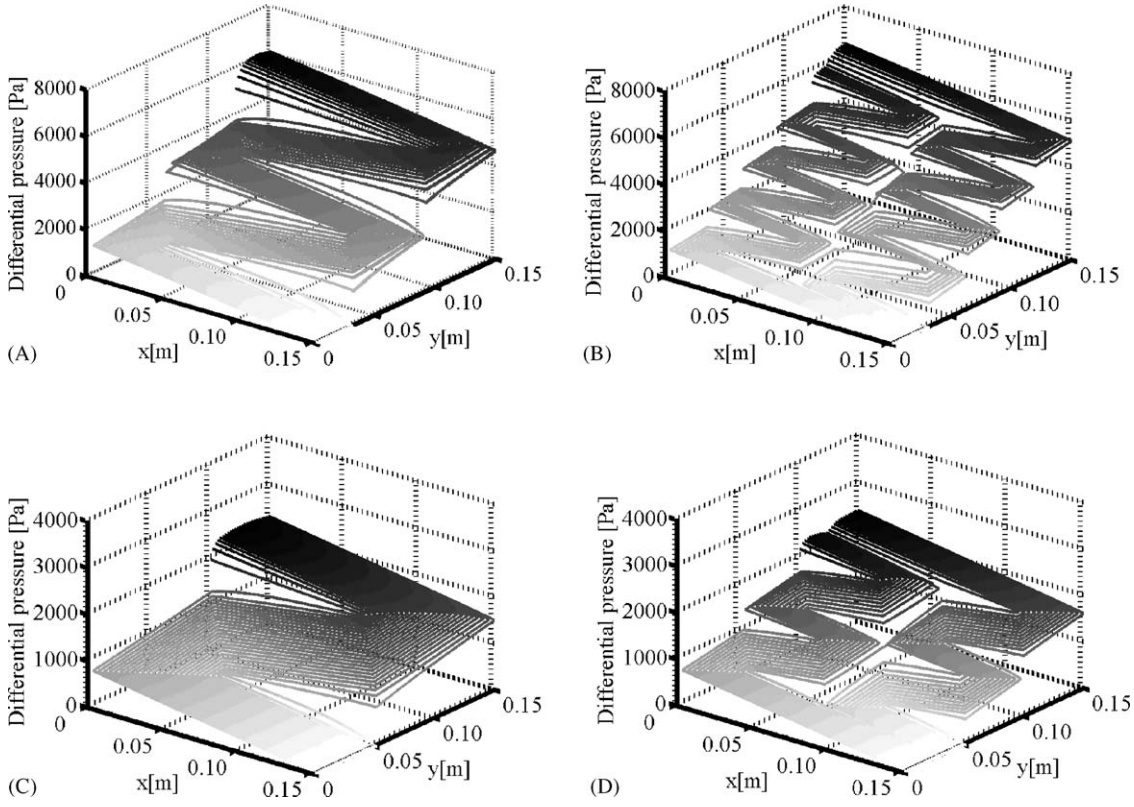

Fig. 15. Pressure distribution with each separator shape (channel depth was 1.0 mm).

distribution uniform. However, there is still disputable point about the other influences caused by increasing the part of elbow, such as the transfer of liquid water. It has not been solved experimentally or numerically yet, so it needs further examinations.

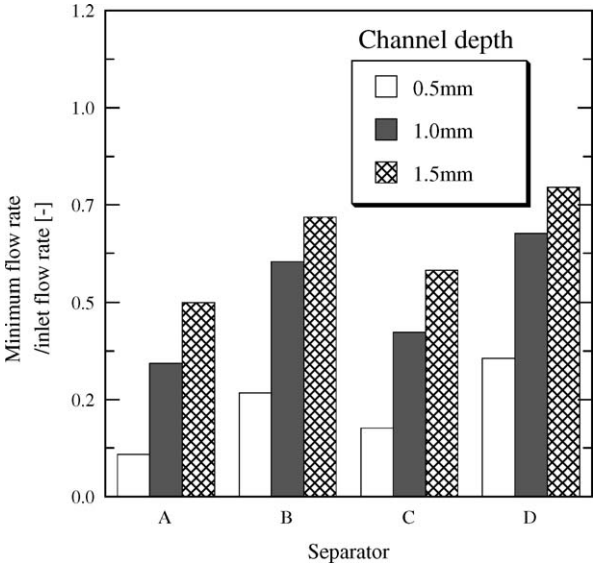

Fig. 16. Effect of separator shape on the rate of the minimum flow velocity to the inlet velocity.

5. Conclusion

The effects of the channel depth, GDL effective porosity, GDL permeability and the cathode gas flow rate on the output performance, the current density distribution and the gas flow condition in an actual scale cell were examined numerically with PEFC reaction and flow analysis model including the oxygen mass transfer model and the gas flow through GDL model which were developed in our former study. Furthermore, the distributed serpentine separator was proposed and the influence of the separator was examined by the numerical analysis. The following results were obtained by these examinations.

1. As a separator channel was shallower, the output density increased. And as the GDL effective porosity was small, the effect of channel depth on the output density increased remarkably. However, the current density distribution with shallow channels was more ununiform than that with deep channels.
2. As the GDL permeability was large, the output density increased. However, the gas flow condition with large GDL permeability transformed to the straight gas flow through GDL from the inlet to the outlet, and the gas flow rate distribution was more remarkable.
3. As the cathode gas flow rate decreased, the effect of channel depth on the output density was reduced. However,

the current density distribution with shallow channels was more ununiform at low gas flow rate condition. Moreover, the rate of the minimum flow velocity to the inlet velocity didn't depend on the gas flow rate.

4. The distributed serpentine separator was effective from the viewpoint of increasing the cell output performance, distributing the current density, and making the gas flow rate distribution uniform.

It was found that channel depth and channel shape affected the output performance, current density distribution and the gas flow condition. On the other hand, because the separator shape also affected the power of supplying gas and the mobility of liquid water in channel, it had to be designed from the comprehensive viewpoint. As this numerical analysis model did not include the effect of the liquid water in channels and GDL in this study, GDL effective porosity and GDL permeability were changed to kinds of parameter. However, when liquid water is stagnant in GDL, it is expected that those can not be separated actually, and that the both values are changed by liquid water. Furthermore, the effect of liquid water, which is not uniform in a cell, and this diffusion inhibition by liquid water must be considered as a local model in an overall cell. In our future study, it is expected that this model will be improved to apply to the various conditions with the influence of liquid water.

Acknowledgement

This research was partially supported by the research and development of polymer electrolyte fuel cell from the New Energy and Industrial Technology Development Organization (NEDO), Japan.

References

[1] A. Hakenjos, H. Muenter, U. Wittstadt, C. Hebling, A PEM fuel cell for combined measurement of current and temperature distribution, and flow field flooding, J. Power Sources 131 (2004) 213–216.
[2] D. Kramer, J. Zhang, R. Shimoi, E. Lehmann, A. Wokaun, K. Shinohara, G.G. Scherer, In situ diagnostic of two-phase flow phenomena in polymer electrolyte fuel cells by neutron imaging. Part A. Experimental, data treatment, and quantification, Electrochim. Acta 50 (2005) 2603–2614.
[3] S. Dutta, S. Shimpalee, J.W. Van Zee, Three-dimensional numerical simulation of straight channel PEM fuel cells, J. Appl. Electrochem. 30 (2000) 135–146.
[4] T. Berning, N. Djilali, Three-dimensional computational analysis of transport phenomena in a PEM fuel cell—a parametric study, J. Power Sources 124 (2003) 440–452.
[5] G. Inoue, Y. Matsukuma, M. Minemoto, Evaluation of the optimal separator shape with reaction and flow analysis of polymer electrolyte fuel cell, J. Power Sources 154 (2006) 18–34.
[6] G. Inoue, Y. Matsukuma, M. Minemoto, Evaluation of the thickness of membrane and gas diffusion layer with simplified two-dimensional reaction and flow analysis of polymer electrolyte fuel cell, J. Power Sources 154 (2006) 8–17.
[7] T.V. Nguyen, A gas distributor for proton-exchange-membrane fuel cells, J. Electrochem. Soc. 143 (1996) 103.
[8] Sukkee Um, C.Y. Wang, Three-dimensional analysis of transport and electrochemical reactions in polymer electrolyte fuel cells, J. Power Sources 125 (2004) 40–51.
[9] H. Dohle, R. Jung, N. Kimiaie, J. Mergel, M. Müller, Interaction between the diffusion layer and the flow field of polymer electrolyte fuel cells—experiments and simulation studies, J. Power Sources 124 (2003) 371–384.
[10] P.H. Oosthuizen, L. Sun, K.B. McAuley, The effect of channel–to-channel gas crossover on the pressure and temperature distribution in PEM fuel cell flow plates, Appl. Therm. Eng. 25 (2005) 1083–1096.
[11] G. Inoue, Y. Matsukuma, M. Minemoto, Effect of Gas Flow through Gas Diffusion Layer on Current Density Distribution of Polymer Electrolyte Fuel Cell, J. Power Sources 157 (2006) 136–152.